Supplementary Figures and Legends

Supplementary Figure 1.

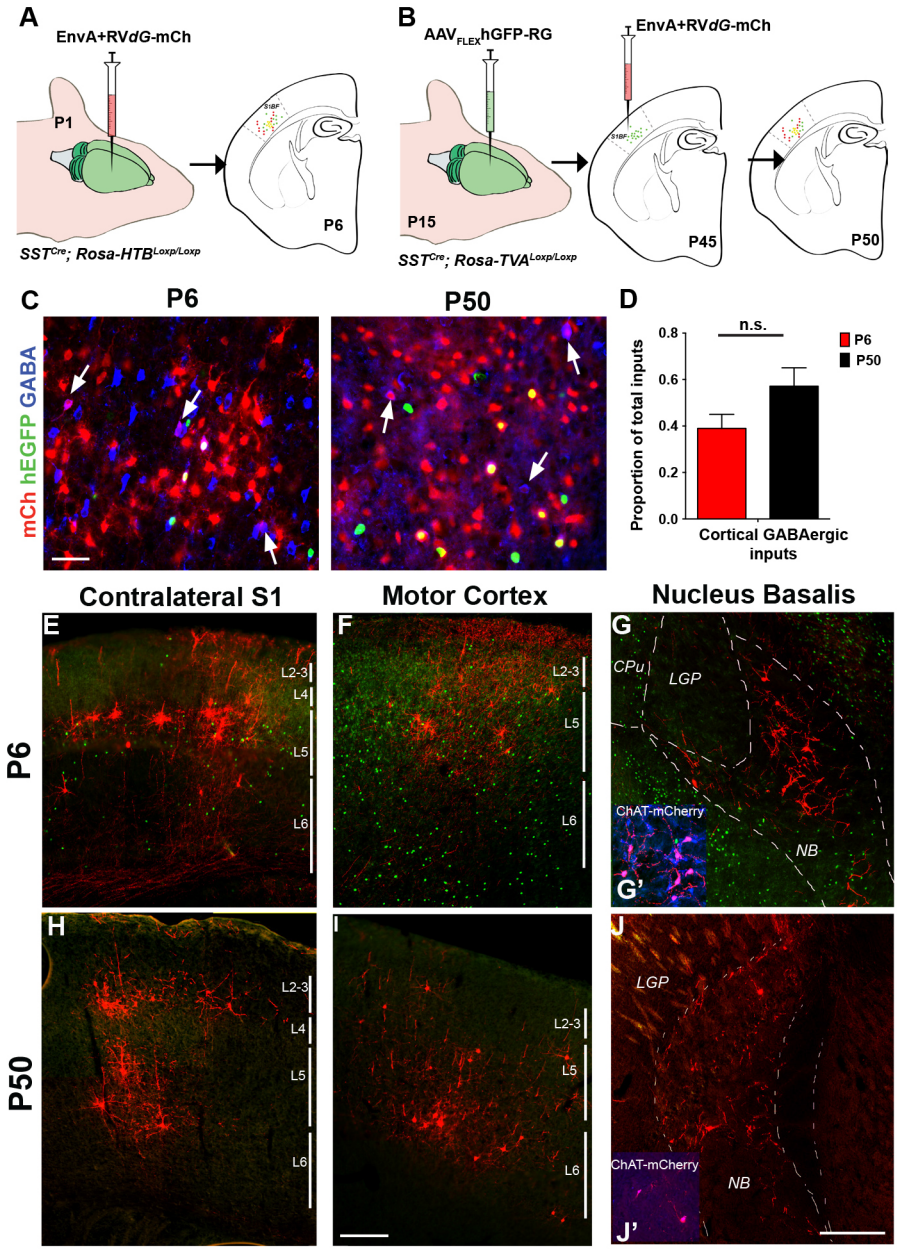

Figure S1, related to Figure 1. Experimental strategy, GABAergic and long-range afferents of SST interneurons. (A) Schematic representation of the experimental strategy for analyzing immature afferent inputs using conditional Rosa-HTB reporter allele with single EnvA+RV*dG*-mCh injection at P1, analysis

was done at P6. (B) Trans-synaptic tracing in older animals by injecting AAV-helper virus at P2 or P15 to animals bearing conditional Rosa-TVA reporter allele, followed by EnvA+RV*dG*-mCh injection to same location 3-4 weeks later, analysis was done 5 days later. (C) Representative images of GABA immunofluorescence in retrograde labeled cells at P6 and P50. All hEGFP expressing neurons were GABA positive and only a small fraction of mCherry expressing neurons were GABA positive. (D) Proportion of local presynaptic neurons expressing GABA protein normalized to number of starter SST interneurons did not show statistically significant difference across the two (n=3 animals each aged P6, P50, n=3 slices closest to the injection region analyzed per animal, Mean ± SEM, $p>0.05$, two-sample t-test, scale bar corresponds to 25μm). Representative images of the afferents inputs arriving from (E,H) contralateral S1, (F,I) motor cortex, (G,J) nucleus basalis. (G',J') Inset images shows immonolabelled ChAT (blue) positive neurons. Scale bars correspond to 100μm.

Supplementary Figure 2.

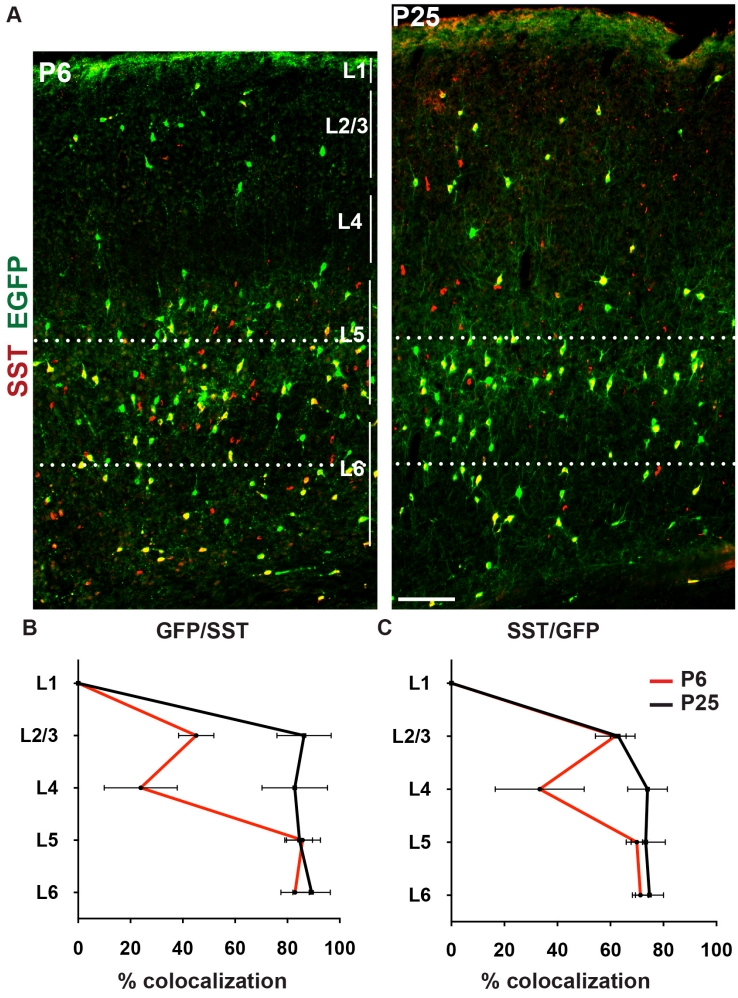

Figure S2 related to Figure 2. Histological verification of EGFP localization to SST expressing cortical interneurons. (A) EGFP and SST immunoflouroscence in the S1BC of *SST*^{CRE}*; RCE*^{EGFP} mice at P6 (left) and P25 (right). The area between the dotted lines mark the thalamorecipient region we sampled for electrophysiology experiments. (B) Percentage of EGFP labeled *SST*^{CRE} neurons that are immunolabelled for SST protein. (C) Percentage of SST positive neurons expressing EGFP Data represent Mean ± SEM, scale bar corresponds to 50μm.

Supplementary Figure 3.

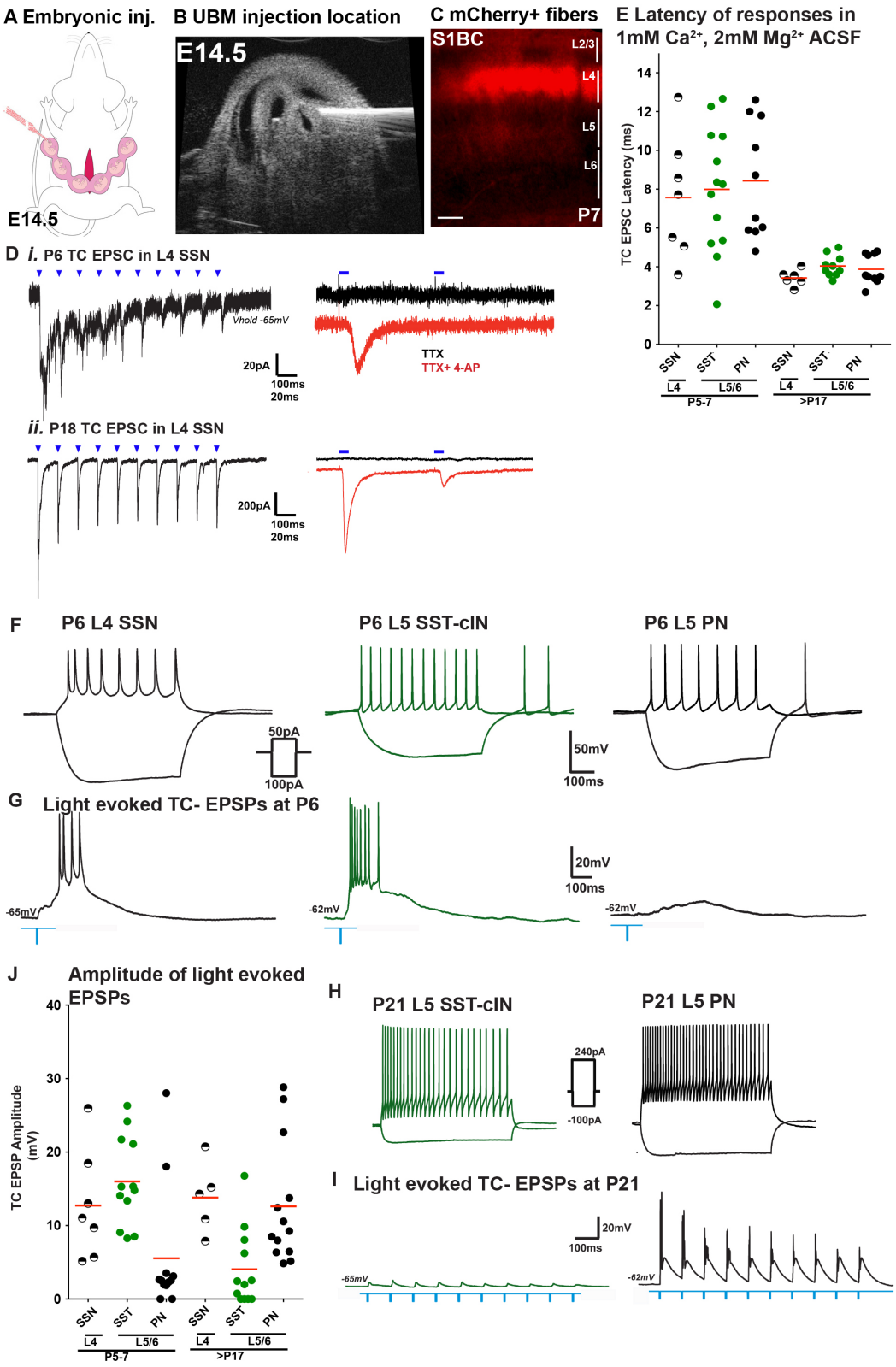

Figure S3 related to Figure 3. Optogenetic activation of thalamic afferents during first and third postnatal weeks. (A) Schematic representation of virus injection surgery in pregnant females. (B) Representative ultrasound image of the injection site in diencephalic primordium of E14.5 embyos, glass needles were targeted dorsolateral to the third ventricle. (C) Representative image of $mCherry^{+}$ fibers in S1 cortex at P7. (D) Representative traces of light evoked thalamic EPSCs in L4 spiny stellate neurons (SSNs) recorded at -65mV holding potential. Note that immature SSNs failed to follow 10Hz stimulation (5ms LED). Traces in right show recording in the presence of TTX alone (black traces) or together with 4-AP (red traces) in P6 (top), and P18 (bottom) L4 SSNs. (E) Population averages of light evoked TC EPSC onset latencies recorded in the presence of low Ca^{2+}/high Mg^{2+} in the ACSF to dampen disynaptic responses. Together, population responses show no significant difference of latencies between cells (L4SSNs, L5/6 SST interneuron, L5/6 PN) in the same age group. (F) Representative membrane potential responses of subgroups of neurons at P6 to the indicated current injections. (G) Representative membrane potential responses of L4 SSN (left), L5/6 SST interneuron (middle), L5/6 PN (right) to 5ms single LED pulse activating thalamic afferents. (H) Representative membrane potential responses of subgroups of neurons at P21 to the indicated current injections. (I) Representative membrane potential responses of L5/6 SST interneuron (left), L5/6 PN (right) to 5ms 10Hz LED pulse activating thalamic afferents. See also Table S2. (J) Population averages of light evoked TC EPSP averages of L4 SSNs and L5/6 SST interneurons and PNs at first and third postnatal week represent similar differences in membrane potential in response to TC activation as shown in TC-EPSCs in Figure 3.

Supplementary Figure 4.

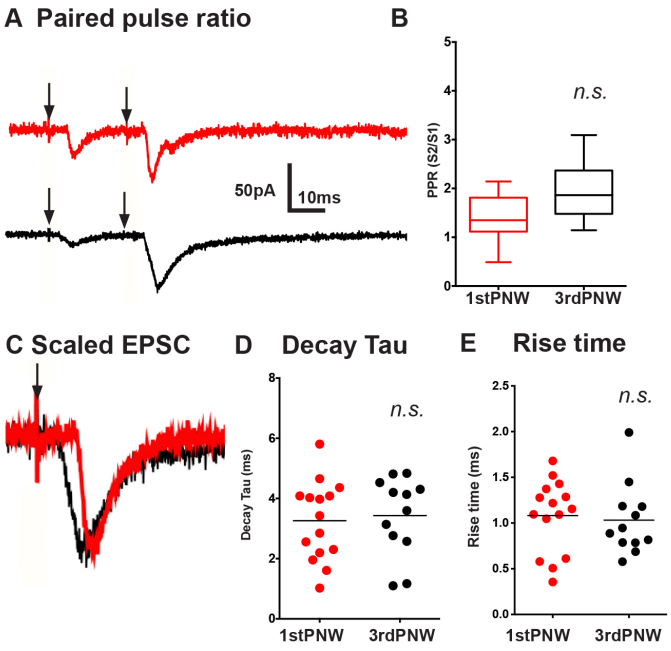

Figure S4 related to Figure 4. Presynaptic release properties and EPSC kinetics of TC inputs on SST interneurons are not altered during development. (A) Example responses from P4 (red), P25 (black) SST interneurons to repetitive TC fiber stimulation (2 pulses, 50Hz) used to calculate paired pulse ratios. (B) Summary plot of whisker (min to max), box (mean) of paired-pulse ratios for SST interneurons recorded at first postnatal week (n=8) and third postnatal week (n=8) show no statistical difference ($p>0.05$). (C) Scaled averaged responses of TC-EPSCs recorded from an example cells. Note the longer onset latency of EPSC recorded in P4 neuron. Population data of (D) decay tau or (E) rise time TC EPSCs on SST interneurons during first postnatal week (n=15) and third postnatal week (n=12) show no statistical difference ($p>0.05$). Data represents mean ± SEM, p values were calculated by Mann-Whitney test.

Supplementary Figure 5.

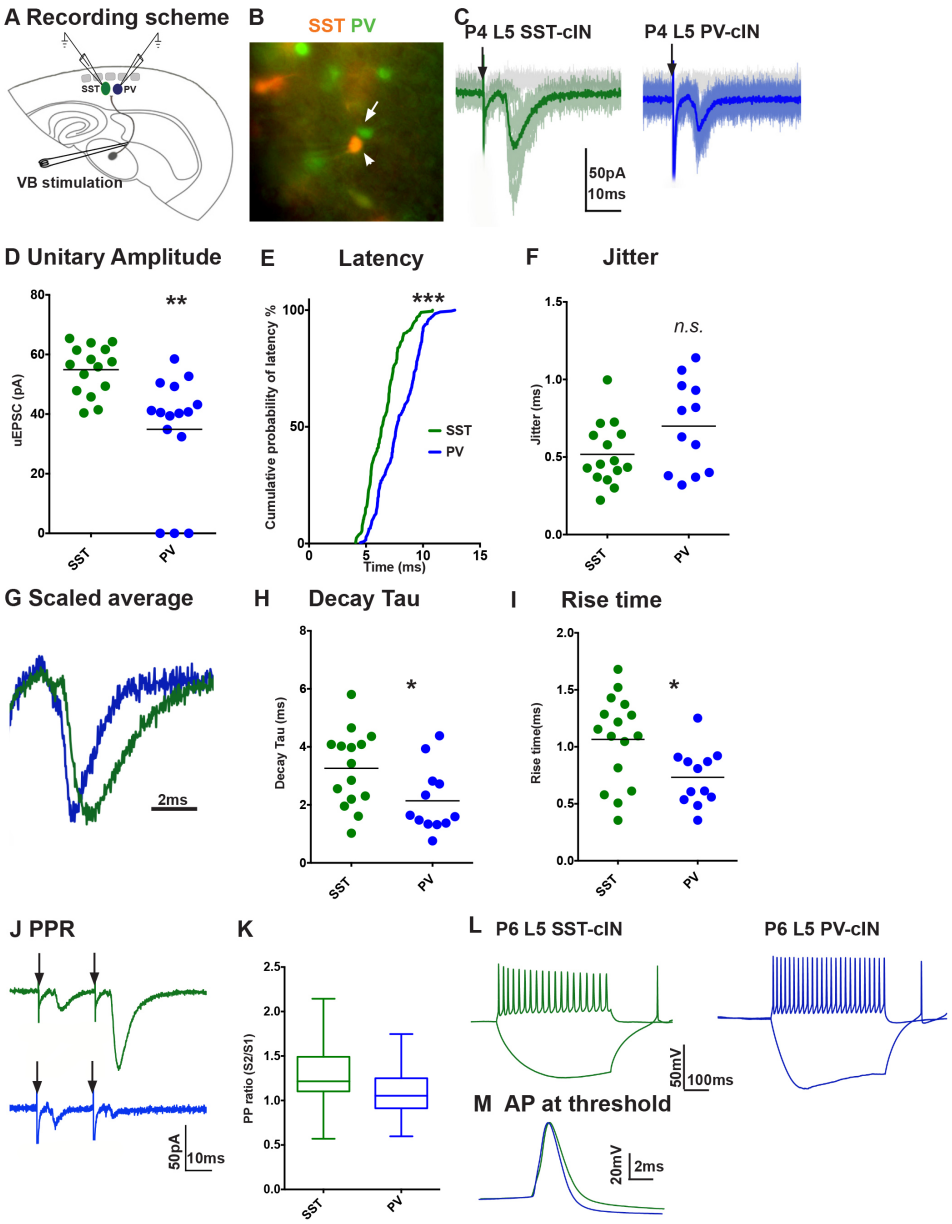

Figure S5 related to Figure 4. During 1st postnatal week, TC responses are weaker in PV interneurons compared to SST interneurons in L5/6 of S1BC. (A) TC evoked synaptic events in SST and PVcINs are recorded in a TC slice preparation at P3-6. (B) SST^{CRE}; Rosa-Ai9^{tdTomato}; Lhx6^{EGFP} genetic cross allowed identification of SST interneurons (arrowhead) and PV interneurons (arrow). (C) Representative traces of EPSCs in SST (green) and PV interneurons (blue) at P4. (D) Excluding failures, peak TC EPSCs in SST interneurons (n=15) was

significantly larger than PV interneurons ($p<0.01$, Mann-Whitney test). We note that the immature SST interneurons recordings were replicated in Figure 4 for comparison. (E). Thalamic EPSC latency was significantly longer in PV interneurons (7.87± 0.1 ms), relative to SST interneurons (6.53 ± 0.1ms, $p<0.0001$, Kolmogorov-Smirnov test). (F) The jitter of latency was not significantly different between two cell types ($p>0.05$, Mann-Whitney test). (F) Scaled average of EPSCs recorded in PV and SST interneurons. (H) Rise and (I) Decay kinetics of PV interneurons was significantly faster than that of SST interneurons ($p<0.05$). $n\geq4$ animals, $n\geq2$ brain slices were analyzed per animal. (J) Example responses to repetitive TC fiber stimulation (2 pulses, 50Hz) used to calculate paired pulse ratios. (K) Summary plot of whisker (min to max), box (mean) of paired-pulse ratios for SST interneurons (n=15) and PV interneurons (n=12) indicating that two cell types have similar PPR ratios ($p>0.05$, mean ± SEM, Mann-Whitney test). (L) Representative membrane potential responses of SST and PV interneurons P6 to current injections, -100pA, 20pA. (M) Overlaid action potentials recorded at threshold current injection in SST and PV interneurons show indistinguishable AP kinetics between two cell types at immature stages. See also Table S2.

Supplementary Figure 6.

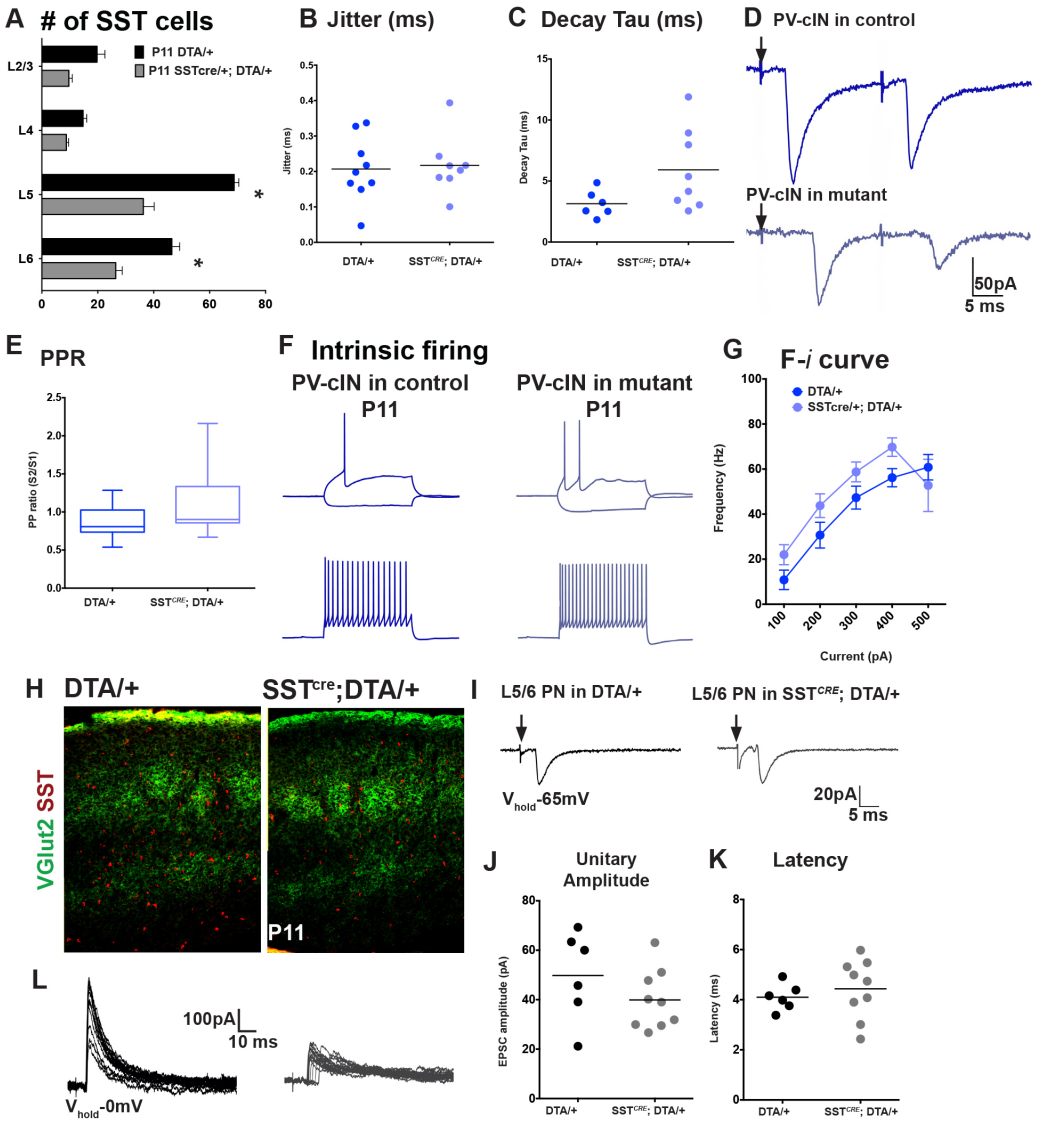

Figure S6 related to Figure 6. Effect of SST interneuron ablation on kinetics and presynaptic release properties of TC-EPSCs and firing properties of PV interneurons and on TC EPSCs and FFI of PNs.

(A) SST interneuron numbers were not further reduced in SST^{CRE}; Rosa-DTA$^{loxp/+}$ mutants compared to Rosa-DTA$^{loxp/+}$ controls at P11. Similar to P5 animals SST interneurons were reduced in L5 and L6 in mutant animals compared to controls ($p<0.001$, n=3 mutant, n=2 control, n≥3 coronal sections were analyzed per animal, two-sample t-test). (B) The latency jitter of TC-EPSCs recorded in PV

interneurons was not significantly different in controls (n=9, 2 animals, 3 slices), compared to mutants (2 animals, 4 slices, $p>0.05$). (C) Population data for decay tau of TC EPSCs indicate a small difference between control and mutant animals that did not reach statistical significance ($p>0.05$). (D) Example responses from PV interneurons in control (dark blue, top), mutant (light blue, bottom) at P11 to repetitive TC fiber stimulation (2 pulses, 50Hz) used to calculate paired pulse ratios. (E) Summary plot of whisker (min to max), box (mean) of paired-pulse ratios for control (n=7) and mutant PV interneurons (n=7, $p>0.05$). (F) Representative membrane potential responses of PV interneurons in control (left), and mutant (right) animals to current injections, -100pA, 100pA (top), 300pA (bottom) (G) Population data representing the averaged F-I curves of PV interneurons control (dark blue) and mutant (light blue). Data represents mean ± SEM, p values were calculated by Mann-Whitney test. (H) Representative image of Vgut2 and SST immunoflouroscence in Rosa-DTA$^{loxp/+}$ control (left panel) and SST^{CRE}; Rosa-DTA$^{loxp/+}$ mutant animals (right panel) shows no visible alteration in TC fiber arborization in the cortex at P11 despite reduction in SST^{+} neurons. (I) Representative traces of averaged EPSCs in PNs in age matched P13 Rosa-DTA$^{loxp/+}$ controls (left) and SST^{CRE}; Rosa-DTA$^{loxp/+}$ mutants (right) evoked by TC fiber stimulation at threshold recorded at -65mV holding potential. (J) Averaged peak amplitude of evoked unitary TC responses in PNs in controls (n=6, 2 animals, 2 slices), and mutants (n=9, 3 animals aged P9-P13, 3 slices, $p>0.05$). (K) Averaged latency was also not significantly different in controls compared to mutants ($p>0.05$). (L) Overlay of IPSCs (Vhold = 0mV) recorded in PNs in control (left) and mutant (right) animals. Data represents mean ± SEM, p values were calculated by Mann-Whitney test.

Supplementary Figure 7.

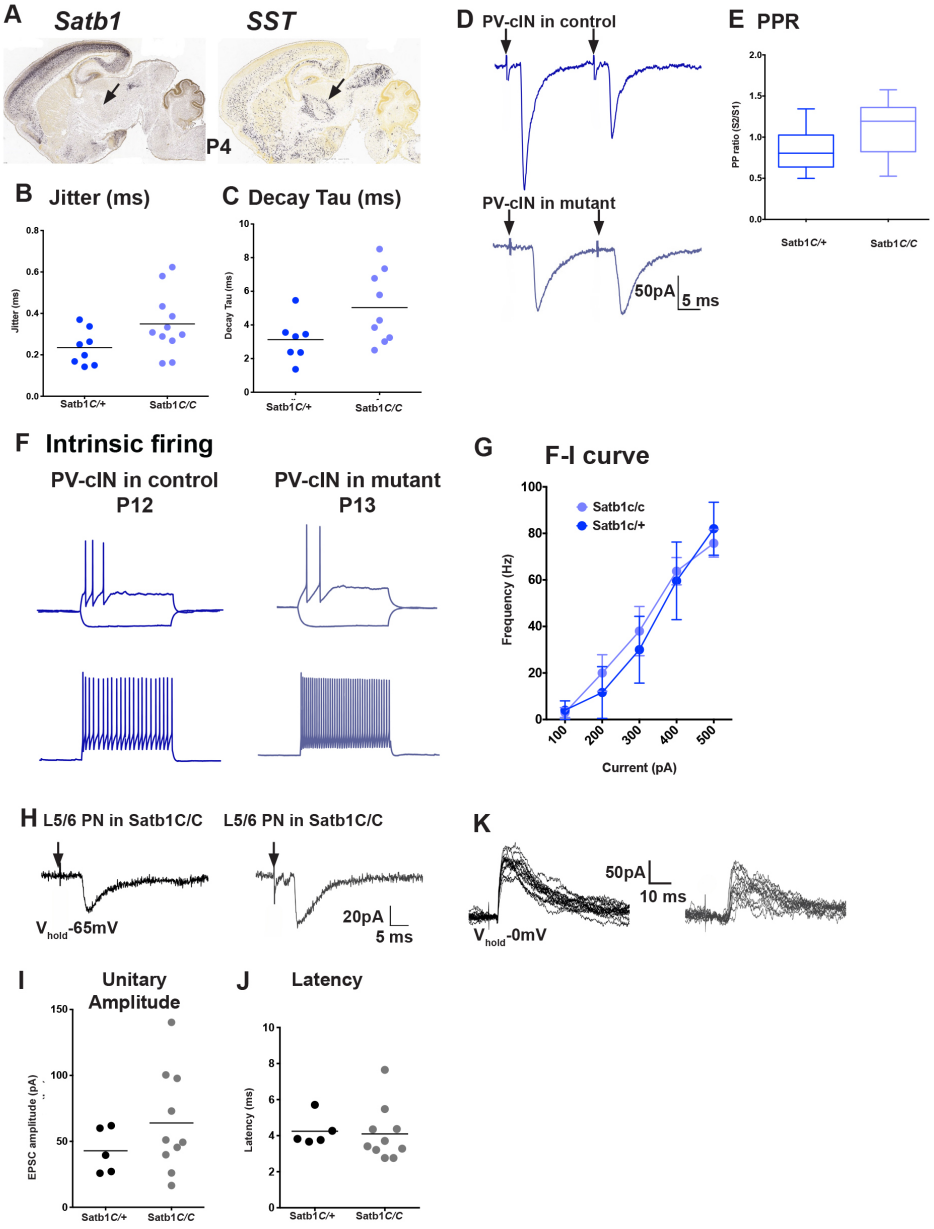

Figure S7 related to Figure 7. Effect of Satb1 loss of function in SST interneurons on kinetics and presynaptic release properties of TC-EPSCs and firing properties of PV interneurons and on TC EPSCs and FFI of PNs.

(A) Representative image of *Satb1* and *Sst* in situ hybridization in P4 animals shows that *Satb1* expression is largely restricted to dorsal telencephalic regions (Website: @2013 Allen Institute for Brain Science). (B) The jitter of latencies of TC-EPSCs recorded in PV interneurons was not significantly different in SST^{CRE};

Rosa-Ai9^{tdTomato}; Satb1$^{C/+}$ controls (n=11, 2 animals, 3 slices), compared to SST^{CRE}; Rosa-Ai9^{tdTomato}; Satb1$^{C/C}$ mutants (3 animals, 4 slices, p>0.05). (C) Population data of the decay tau of TC EPSCs in PV interneurons in control and mutant animals did not reach statistical significance (p>0.05). (D) Example responses from PV interneurons in control (dark blue, top), mutant (light blue, bottom) at P12, and P13 respectively to repetitive TC fiber stimulation (2 pulses, 50Hz) used to calculate paired pulse ratios. (E) Summary plot of whisker (min to max), box (mean) of paired-pulse ratios for control (n=11) and mutant PV interneurons (n=7, p=0.08). (F) Representative membrane potential responses of PV interneurons in control (left), and mutant (right) animals to current injections, -100pA, 100pA (top), 300 pA (bottom). (G) Population data representing the averaged F-I curves of PV interneurons control (dark blue, n=5) and mutant (light blue, n=8, p values for all data points: p>0.05). Data represents mean ± SEM, p values were calculated by Mann-Whitney test. (H) Representative traces of averaged EPSCs in PNs in age matched P14 SST^{CRE}; Rosa-Ai9^{tdTomato}; Satb1$^{C/+}$ controls, compared to SST^{CRE}; Rosa-Ai9^{tdTomato}; Satb1$^{C/C}$ mutants evoked by TC fiber stimulation at threshold recorded at -65mV holding potential. (J) Averaged peak amplitude of evoked unitary TC responses in PNs in controls (n=5, 2 animals, 3 slices), and mutants (n=10, 3 animals, 5 slices, p>0.05). (K) Averaged latency was also not significantly different in controls compared to mutants (p>0.05). (L) Overlay of IPSCs (Vhold = 0mV) recorded in PNs in control (left) and mutant (right) animals. P values were calculated by Mann-Whitney test.

Supplementary Figure 8.

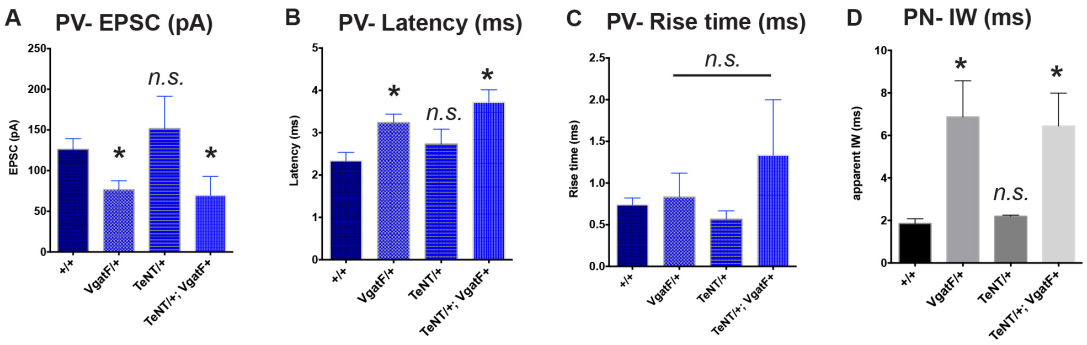

Figure S8 related to Figures 6-8. Genetic manipulations of SST interneurons synaptic outputs. EPSC amplitude (A), latency (B), and rise time (C) of evoked TC responses in PV interneurons in controls (n=7, 4 slices, animals aged P12,14,16), *SST*^{CRE};*Vgat*$^{C/+}$mutants (n=7, 5 slices, animals aged P13,16, 19), *SST*^{CRE};Rosa-TeTN mutants (n=4, 2 slices, animals aged, P13, 5), and *SST*^{CRE};RosaTeTN;*Vgat*$^{C/+}$compound mutants (n=7, 5 slices, animals aged P12,13,14). (D) Averaged IW of PNs in controls (n=5), and mutants (n=7,4,7), indicating feed-forward inhibition recorded in PNs. Data represent mean ± SEM, p values are calculated by pair-wise Mann-Whitney test by comparing each mutant to the control.

Table S1, related to Figure 1. Number of starter SST interneurons analyzed in retrograde tracing experiments.

The number of EnvA+RV*dG*-mCh and hEGFP coexpressing starter neurons, with corresponding laminar location is given for each brain we used for the analysis of cortical and subcortical retrograde afferents to SST interneurons during development. Values shown are expressed as mean ± SEM.

Supplementary Table 1. Number of starter SST interneurons analyzed in retrograde tracing experiments

Animal	Genotype	Day of AAV-B19 inj	Day of RV inj	Day of analysis	# SST L2/3	# SST L4	# SST L5	# SST L6
P1	SSTcre:HTB	-	P1	P6	14	8	68	47
P2	SSTcre:HTB	-	P1	P6	4	5	51	80
P3	SSTcre:HTB	-	P1	P6	10	6	89	57
P4	SSTcre:HTB	-	P1	P6	0	3	10	68
P3	SSTcre:HTB	-	P1	P6	0	4	19	31
				Mean ± SEM	**5.6 ± 2.8**	**5.2 ± 1.9**	**47.4 ± 14.78**	**56.6 ± 8.4**
A1	SSTcre:TVA	P15	P45	P50	26	27	86	49
A2	SSTcre:TVA	P15	P45	P50	25	19	72	44
A3	SSTcre:TVA	P15	P45	P50	3	21	24	23
A4	SSTcre:TVA	P15	P45	P50	13	11	22	17
A5	SSTcre:TVA	P15	P45	P50	6	7	43	67
M1	SSTcre:TVA	P2	P25	P30	0	3	35	53
M2	SSTcre:TVA	P2	P25	P30	0	1	28	48
				Mean ± SEM	**10.4 ± 4.2**	**13 ± 3.7**	**44 ± 9.4**	**43 ± 6.57**

Table S2, related to Figures 3,4,S5. Electrophysiological Parameters of Subgroups of Neurons in Somatosensory Cortex

Intrinsic membrane properties of neurons at 1st postnatal week (SST interneuron, n=12, PN, n=11, PV interneuron, n=15) and at 3rd postnatal week (SST interneuron, n=18, PN, n=11) were characterized by applying hyperpolarizing and depolarizing steps of 500-ms duration were applied in 20 or 2pA increments at 0.125 Hz as described previously (Xu et al., 2013). Values shown are expressed as mean ± SEM, p values were calculated by two-sample t-test. Significant differences between 1st postnatal week SST interneurons and PNs are expressed as (*), between 1st postnatal week SST interneurons and PV interneurons are expressed as ($^{+}$), between 3rd postnatal weekSST interneurons and PNs are expressed as ($^{\#}$).

Supplementary Table 2. Electrophysiological Parameters of Subgroups of Neurons in Somatosensory Cortex

	1st PNW SST	1st PNW PN	1st PNW PV	3rd PNW SST	3rd PNW PN
Vrest (mV)	-49.63 ± 1.16	-57.59 ± 2.52*	-47.97 ± 1.62$^{\cdot}$	-62.46 ± 1.53	-68.29 ± 1.51$^{\#}$
Rin (mΩ)	579.20 ±31.79	422.70 ± 19.60**	667.69 ± 81.22^{+}	203.10 ± 16.19	193.59 ± 12.60
τ (ms)	54.37 ± 5.00	41.71 ± 2.86	55.52 ± 3.47	19.25 ± 1.64	18.45 ± 1.63
Rheobase (pA)	10.00 ± 3.78	22.57 ± 6.19	9.00 ± 1.34	74.95 ± 12.54	119.00 ± 19.65
Threshold (mV)	-32.45 ± 1.59	-28.46 ± 1.58	-29.00 ± 1.08	-43.04 ± 0.98	-39.09 ± 0.87$^{\#}$
Spike width (mV)	1.68 ± 0.07	1.59 ± 0.10	1.59 ± 0.08	0.60 ± 0.04	0.92 ± 0.07$^{\#\#}$
Time to AHP	23.91 ± 2.47	42.51 ± 6.99	17.96 ± 1.69	2.49± 0.24	14.17 ± 3.74$^{\#}$
AHP amplitude	15.08 ± 0.98	17.72 ± 1.86	20.84 ± 1.00^{+++}	14.62 ± 1.51	19.00 ± 2.35
Fmax steady-state (Hz)	37.85 ± 2.30	25.76 ± 2.32**	55.63 ± 3.11^{+++}	75.92 ± 6.19	40.82 ± 9.70$^{\#\#}$
Fmax initial (Hz)	63.36 ± 3.13	44.58 ± 2.76	76.51 ± 4.26	162.40 ± 9.69	88.72 ± 15.04$^{\#\#\#}$
Spike adaptation ratio	40.02 ± 2.16	42.82 ± 2.17	26.90 ± 2.02^{+++}	53.15 ± 2.64	50.04 ± 5.63

Supplemental Experimental Procedures

Mouse Strains

SST^{CRE} (Taniguchi et al., 2011), *Rosa-HTB* (Li et al., 2013), *Rosa-TVA* (Seidler et al., 2008), *RCE*^{EGFP} (Sousa et al., 2009), *Lhx6*^{EGFP} (Gong et al., 2003), *Rosa-Ai9*^{tdTomato}, *Rosa-Ai32*^{ChR2} (Zariwala et al., 2012), *Rosa-DTA* (Voehringer et al., 2008), *Satb1* conditional (Close et al., 2012), Rosa-TeNT (Zhang et al., 2008) , Vgat conditional (Tong et al., 2008) mouse strains, including genotyping protocols have been described previously.

Virus injections for retrograde tracing experiments

RV-mCh titers were set to titers ~1e10^{8} for retrograde tracing experiments and were 1:500 diluted for SST interneurons reconstruction experiments. S1BC in P1 *SST*^{CRE}*-Rosa-HTB* animals were targeted using a custom made mold by empirically determined coordinates using transverse sinus and superior sagittal sinus as reference (typical coordinate: 1.5mm anterior from transverse sinus, 1.9mm lateral to superior sagittal sinus, at a 0.35mm depth from surface). Animals were anaesthetized by inducing hypothermia on ice and kept on either ice-cold clay mold. The dura was exposed by making a small incision through the skin and thin skull. 50nL of virus diluted in HBSS was delivered using a beveled glass micropipette (tip diameter ~20mm) attached to a Nanoliter 2000 pressure injection apparatus (World Precision Instruments), over a 2 min period, the pipette was held in place for 3 min following each injection before retraction from the brain. Animals were kept at 37C for 2-3 hours before being return to dam. *SST*^{CRE}*-Rosa-TVA* mice, aged between P10-15 were anesthesized with 2% isoflurane and placed in stereotaxic frame (Kopf, Model 1900). Helper adeno-

associated virus (100nL) carrying fusion gene for Rabies glycoprotein B19 (*AAV1/2.EF1a.FLEX.hGFP.B19G*; Gene Transfer, Targeting and Therapeutics Core, Salk Institute) (Sun et al., 2014) was delivered to coordinates 0.8mm posterior to Bregma; 3.6 mm lateral to the midline, at a depth of 0.9mm from the cortical surface. Animals were returned to home cage until P45, at which time 100nL of RV-mCherry was delivered to the same coordinates. Animals were anesthetized by intraperitoneal injection of Sleepaway (0.1 mg/g body weight) followed by transcardiac perfusion of 4% paraformaldehyde in PBS for immunohistochemistry analysis.

A**nalysis of presynaptic inputs by Rabies tracing**

All cryostat sections from an individual rabies infected brain were collected, one out of six sections was used for examination and quantification of starter neurons, as well as the presynaptic cells in different brain structures that projected to them. All sections of the brain containing mCherry fluorescent signal were collected and matched with a corresponding anatomical location, and layer. Starter cells were identified based on mCherry and hGFP coexpression, and presynaptic cells were identified based on mCherry expression. The reported number of starter cells corresponds to $1/6^{th}$ of all cells labeled in each brain (as we only examined every sixth section). Presynaptic inputs originating from cortex are expressed as the percentage of cells locate in each cortical layer, and inputs originating from long range afferents are expressed as the total number of $mCherry^{+}$ neurons in each region divided by the number starter cells which indicated the proportion of presynaptic cells. We observed that, when the mice

was inoculated at P10 and analyzed 5 days later, mCherry expression was restricted to the SST expressing population (i.e. h-EGFP expressing) and we observed very little trans-neuronal spread ($mCherry^+$ cells) from initially infected SST interneurons. Longer post-inoculation times did not improve the degree of trans-neuronal labeling. We reasoned that lack of transsynaptic labeling at this age is likely due to insufficient expression of rabies glycoprotein transgene from the Rosa locus. Consequently, cells fail to complement the G deleted RV-mCherry, and hence are unable to produce infectious particles. Hence, we performed adult tracing experiments with dual injections of AAV-helper virus and RV-mCherry.

Antibodies

Cryostat tissue sections (25 μm) were stained with the following primary antibodies: rat anti-EGFP (1:1000, Nacalai Tesque), chicken anti-EGFP (1:1000, Aves labs), rabbit anti-DsRed (1:500, Milllipore), rat anti-RFP (1:500, Allele Biotech), rat anti-somatostatin (1:250; Chemicon), guinea-pig anti-Vglut2 (1:10.000, Millipore), rabbit anti-GABA (1:500, Sigma). Secondary antibodies used were conjugated with Alexa fluorescent dyes 488, 594, 647 (Molecular Probes), nuclear counterstaining was performed with 100 ng/ml 4,6-diamidino-2-phenylindole (DAPI) solution in PBS for 5 min.

EdU histochemical analysis

Timed-pregnant females at E10.5 were given 3 pulses of EdU during 12 hours (5mg/kg intraperitoneally), litter was sacrificed on P6 and P25, and brains were processed for EdU-GFP double immunofluorescent labeling according to

manufacturer's instructions (Clik-iT Alexa Fluor 594 Imaging kit, Molecular Probes). For each animal analyzed, images from five somatosensory cortex sections normalized to 1mm^2 by ImageJ were used to assist the conversion of pixel^2 to mm^2 to count cell numbers. Changes in SST interneuron numbers at P6 and P25, which are generated at E10.5 was reported as proportion of EdU-EGFP double labeled cells divided by total EGFP$^+$ cells at each section. Since cell density decreases during development due to a concomitant increase in cortical volume (between P6-P25, ~30-40% increase, data not shown), we sectioned P6 brains at 15μm thickness and P25 brains at 20μm thickness to obtain same number of coronal sections containing S1BC.

Synaptic Puncta Analysis

Animals were perfused as described above. Cryostat sections 16 μm were blocked for 1 hour in 10% donkey serum PBS with 0.1% triton100-X (PBST) and incubated overnight at 4C^0 with the following primary antibodies: chicken anti-EGFP (1:1000, Abcam), guinea pig anti-Vglut2 (1:500, Synaptic Systems), and guinea pig anti-Vglut1 (1:500, Synaptic Systems). Sections were then washed 4 times with PBST, incubated for 1 hour at room temperature with secondary Alexa-conjugated antibodies (1:1000, Invitrogen), washed 4 times with PBST and then mounted with Flouromount G (Southern Biotech). Images were taken within the deep layers of the somatosensory cortex of at least three different sections from three different animals per age with a Zeiss LSM 510 laser scanning confocal microscope. Scans were performed to obtain 4-5 optical Z sections of 0.33 μm each (totaling ~1μm thickness image maximal projection) with a 63x/1.4

Oil DIC objective. The same scanning parameters (i.e. pinhole diameter, laser power/offset, speed/averaging) were used for all images. Maximum projections of 4-5 consecutive 0.33μm optical sections were analyzed with ImageJ (NIH) puncta analyzer plugin to count for the number of puncta consisting of co-localized pre-synaptic marker and post-synaptic SST cell soma and proximal dendrites. Average synaptic puncta density per image was normalized to total fluorescent area (pixel^2) scanned for each condition. Puncta Analyzer plugin is written by Bary Wark, and is available for download (https://github.com/physion/puncta-analyzer).

Virus injections

A detailed description of ultrasound backscatter-guided transplantation has been described elsewhere (Nery et al., 2002; Wichterle et al., 2001). Briefly, AAV suspension carrying *AAV2/1.CAG. hChR2(H134R)-mCherry.WPRE.SV40* (Addgene20938M, Upenn Vector Core) were frontloaded into a pulled and beveled glass pipette (tip diameter ~20mm) attached to a micromanipulator (Narishige MO-10) and delivered into the diencephelon of E14.5 embryos using ultrasound-guided backscatter microscopy with the Vevo 770 system (VisualSonics, 40 MHz probe 704). Following surgery, the uterus was carefully replaced, and the dam was sutured, allowing pups to be born normally. To facilitate successful injections, embryos are obtained from *SST*$^{CRE/CRE}$, *RCE*$^{EGFP/EGFP}$ homozygous cross. Animals were sacrificed from P5 onward for slice electrophysiology.

Postnatal injections were performed similar to the protocol used for

retrograde injections. Empirically determined coordinate for prenatal VB thalamic nucleus was 0.2 mm anterior from transverse sinus, 1.2 mm lateral to superior sagittal sinus, at a 2 mm depth from surface. 15-25nL of *AAV2/1.CAG. hChR2(H134R)-mCherry.WPRE.SV40* was injected bilaterally. P2 cortical injection *of AAV2/1.Flex.EF1a.hChR2(H134R)-mCherry.WPRE.SV40* (Addgene20297, Upenn Vector Core) and P1 cortical injection of *AAV2/1-Flex.DTR.GFP* (gift from T. Jessel) were similar to the injection of EnvA+RV*dG*-mCh in retrograde tracing experiments described above using same coordinates. Slice physiology experiments were conducted 5-6 days after ChR2 injection. 400ng of DT was administered intraperitoneally on P8, followed by recordings between P13-P17.

Brain slice preparation

Animals were anesthetized by intraperitoneal injection of Sleepaway (0.1 mg/g body weight) followed by decapitation of immature animals. Older animals were transcardially perfused with ~20 ml ice-cold sucrose-ACSF solution containing (in mM) 87 NaCl, 75 Sucrose, 2.5 KCl, 1.25 NaH_2PO_4, 26 $NaHCO_3$, 10 Glucose, 1 $CaCl_2$, 2 $MgCl_2$. The brain was quickly removed and immersed in ice-cold oxygenated sucrose cutting solution. Coronal slices (300μm) or thalamocortical slices (350 μm thick in immature animals, 400 μm in mature) through primary somatosensory cortex were generated as previously described (Agmon and Connors, 1991; Kruglikov and Rudy, 2008) using a Leica VT 1000S vibratome and recovered in a holding chamber at 32^0C for 30 min and at room temperature for 30 min prior to physiological recordings. For recordings a slice

was transferred to ACSF contained (in mM) 125 NaCl, 20 Glucose, 2.5 KCl, 1.25 NaH_2PO_4, 26 $NaHCO_3$, 2 $CaCl_2$, 1 $MgCl_2$, perfused in recording chamber 8 ml/min at 32^0C. All slice preparation and recording solutions were oxygenated with carbogen gas (95% O_2, 5% CO_2, pH 7.4). To facilitate recording monosynaptic responses we occasionally altered Ca/Mg concentrations to 1 $CaCl_2$, 2 $MgCl_2$, but this did not have a substantial effect on the amplitude or latency of responses.

Electrophysiological Recordings

Whole-cell patch-clamp recordings were obtained from EGFP, tdTomato expressing interneurons or non-fluorescent pyramidal shaped neurons that were located adjacent to the sampled interneuron. Patch electrodes (3–6 MΩ) were pulled from borosilicate glass (1.5 mm OD, Harvard Apparatus). For all recordings the patch pipettes were filled with a solution containing (in mM): 130 K-gluconate, 0.5 EGTA, 7 KCl, 10 HEPES, 4 Mg-ATP, 0.3 Na-GTP, 5 tris-phosphocreatine (pH 7.2 with KOH) and 0.3% biocytin (Tocris). The predicted E_{Cl} under these conditions was ~-70mV. During patching, cell attached series resistances were >1GΩ and series resistance after achieving whole-cell configuration was between 10-30MΩ. Membrane potentials were not corrected for liquid junction potential and access resistance was not compensated. Resting membrane potential measurement was made immediately after breaking into the cell, and a series of hyperpolarizing and depolarizing step currents were injected to measure the intrinsic properties of each neuron, only cells with stable series resistance (<20% change throughout the recording) were used for analysis.

Holding potentials were -65mV for experiments involving whole-cell voltage clamp experiments testing excitatory postsynaptic currents, 0mV for inhibitory postsynaptic currents, -45mV to obtain EPSC/IPSC sequences. When a cell-attached configuration was used, the pipette was set at 0mV. To activate thalamic afferents, extracellular stimuli were delivered using tungsten bipolar stimulating electrode placed on axons exiting VB. Stimulation intensities were chosen to be just above the threshold (range 20–500 μA). Data were collected using a Multiclamp 700B amplifier (Molecular Devices), digitally sampled at 20 kHz and low-pass filtered at 5 kHz (Digidata 1440A, Molecular Devices), pClamp 10 software was used for data acquisition. Following drugs (Tocris) were used where indicated: TTX (1 mM), 4-Aminopyridine (800 mM), SR95531 (20 μM), D-AP5 (50 μM), NBQX (20 μM). For optical stimulation experiments the light duration used with the BioLED in the presence of TTX and 4-AP was set to 10-50ms to get optimal responses from immature slices in all cell types recorded.

Electrophysiological analysis

Data analysis was performed off-line using the Clampfit module of pClamp (Molecular Devices), Prism 5 (GraphPad Software), and Microsoft Excel suites of programs. Intrinsic membrane properties of neurons were characterized by applying hyperpolarizing and depolarizing steps of 500-ms duration were applied in 20 or 2pA increments at 0.125 Hz as described previously (Xu et al., 2013). The amplitude of evoked synaptic values were obtained by measuring the peak amplitude of individual waveforms and subsequently averaged. A minimum of 10 individual waveforms were used for optical experiments, 30 for electrical

stimulation and the number of cells examined is notified within the figure legends. The latency was measured individually as time between the beginning light onset or the deflection of the electrical stimulus artifact and the onset of the synaptic current. Jitter was calculated as the standard deviation of latency. The charge was calculated as area, measured as an absolute value of the integral of the synaptic current. The decay time was calculated by fitting the individual traces with a single (SST interneuron events in immature and mature, PV interneuron immature) or double exponential (PV interneurons in second postnatal week). If the events were best fit with biexponential decay, the amplitude-weighted average EPSC decay time constant was determined by measuring τ_1, τ_2, from individual events, τ_1, τ_2, being weighted with their respective fractional amplitude contributions.

Neuronal reconstruction

To visualize morphology of immature SST interneurons, ~1:500 diluted RV-mCherry was injected to the S1BC of *SST^{CRE};Rosa-TVA* P1 animals as described previously, brains were sectioned (300μm thick), immunostained. Alternatively, recording slices containing biocytin filled cells after a recording day were fixed with 4% paraformaldehyde in PBS for 1-2 hours, rinsed with PBS, and incubated in blocking solution containing 1% BSA, 10% NDS, 0.5% Triton-X, 0.2% fish gelatin in PBS for 2h. Slices were then incubated with streptavidin conjugated Alexa488 alone or together with rat anti-SST (for *post-hoc* identification) overnight in 4^{0}C in diluted (1:10) blocking solution. Slices were then repeatedly washed with diluted blocking solution prior to incubation with

secondary antibodies for 2h room temperature. After washing 3-4 times with diluted blocking solution and PBS sections were mounted on glass slides with Vectashield (Vector Laboratories) and coverslipped. Flourescently labeled neurons were imaged and reconstructed using Zeiss510 Meta confocal microscope and Neurolucida software (MicroBrightField).

Supplementary References

Agmon, A., and Connors, B.W. (1991). Thalamocortical responses of mouse somatosensory (barrel) cortex in vitro. Neuroscience 41, 365-379.

Close, J., Xu, H., De Marco Garcia, N., Batista-Brito, R., Rossignol, E., Rudy, B., and Fishell, G. (2012). Satb1 is an activity-modulated transcription factor required for the terminal differentiation and connectivity of medial ganglionic eminence-derived cortical interneurons. J Neurosci 32, 17690-17705.

Gong, S., Zheng, C., Doughty, M.L., Losos, K., Didkovsky, N., Schambra, U.B., Nowak, N.J., Joyner, A., Leblanc, G., Hatten, M.E., and Heintz, N. (2003). A gene expression atlas of the central nervous system based on bacterial artificial chromosomes. Nature 425, 917-925.

Kruglikov, I., and Rudy, B. (2008). Perisomatic GABA release and thalamocortical integration onto neocortical excitatory cells are regulated by neuromodulators. Neuron 58, 911-924.

Li, Y., Stam, F.J., Aimone, J.B., Goulding, M., Callaway, E.M., and Gage, F.H. (2013). Molecular layer perforant path-associated cells contribute to feed-forward inhibition in the adult dentate gyrus. Proceedings of the National Academy of Sciences of the United States of America 110, 9106-9111.

Nery, S., Fishell, G., and Corbin, J.G. (2002). The caudal ganglionic eminence is a source of distinct cortical and subcortical cell populations. Nat Neurosci 5, 1279-1287.

Seidler, B., Schmidt, A., Mayr, U., Nakhai, H., Schmid, R.M., Schneider, G., and Saur, D. (2008). A Cre-loxP-based mouse model for conditional somatic gene expression and knockdown in vivo by using avian retroviral vectors. Proceedings of the National Academy of Sciences of the United States of America 105, 10137-10142.

Sousa, V.H., Miyoshi, G., Hjerling-Leffler, J., Karayannis, T., and Fishell, G. (2009). Characterization of Nkx6-2-derived neocortical interneuron lineages. Cereb Cortex 19 Suppl 1, i1-10.

Sun, Y., Nguyen, A.Q., Nguyen, J.P., Le, L., Saur, D., Choi, J., Callaway, E.M., and Xu, X. (2014). Cell-type-specific circuit connectivity of hippocampal CA1 revealed through Cre-dependent rabies tracing. Cell reports 7, 269-280.
Taniguchi, H., He, M., Wu, P., Kim, S., Paik, R., Sugino, K., Kvitsiani, D., Fu, Y., Lu, J., Lin, Y.*, et al.* (2011). A resource of Cre driver lines for genetic targeting of GABAergic neurons in cerebral cortex. Neuron 71, 995-1013.
Tong, Q., Ye, C.P., Jones, J.E., Elmquist, J.K., and Lowell, B.B. (2008). Synaptic release of GABA by AgRP neurons is required for normal regulation of energy balance. Nat Neurosci 11, 998-1000.
Voehringer, D., Liang, H.E., and Locksley, R.M. (2008). Homeostasis and effector function of lymphopenia-induced "memory-like" T cells in constitutively T cell-depleted mice. Journal of immunology 180, 4742-4753.
Wichterle, H., Turnbull, D.H., Nery, S., Fishell, G., and Alvarez-Buylla, A. (2001). In utero fate mapping reveals distinct migratory pathways and fates of neurons born in the mammalian basal forebrain. Development 128, 3759-3771.
Xu, H., Jeong, H.Y., Tremblay, R., and Rudy, B. (2013). Neocortical somatostatin-expressing GABAergic interneurons disinhibit the thalamorecipient layer 4. Neuron 77, 155-167.
Zariwala, H.A., Borghuis, B.G., Hoogland, T.M., Madisen, L., Tian, L., De Zeeuw, C.I., Zeng, H., Looger, L.L., Svoboda, K., and Chen, T.W. (2012). A Cre-dependent GCaMP3 reporter mouse for neuronal imaging in vivo. J Neurosci 32, 3131-3141.
Zhang, Y., Narayan, S., Geiman, E., Lanuza, G.M., Velasquez, T., Shanks, B., Akay, T., Dyck, J., Pearson, K., Gosgnach, S.*, et al.* (2008). V3 spinal neurons establish a robust and balanced locomotor rhythm during walking. Neuron 60, 84-96.